Journal of Membrane Science 493 (2015) 28–36

Contents lists available at ScienceDirect

Journal of Membrane Science

journal homepage: www.elsevier.com/locate/memsci

Acid blue 9 desalting using electrodialysis

Chang Xue [a], Qing Chen [a], Yuan-Yuan Liu [a], Yu-Ling Yang [a], Dan Xu [b], Lixin Xue [c], Wei-Ming Zhang [a,*]

[a] College of Chemistry & Materials Engineering, Wenzhou University, Wenzhou 325000, PR China
[b] Hubei Sanjiang Hongyang Co. Ltd., Xiaogan 432000, PR China
[c] Key Laboratory of Marine Materials and Related Technologies, Chinese Academy of Sciences, and Zhejiang Key Laboratory of Marine Materials and Protective Technologies, Ningbo 315201, PR China

ARTICLE INFO

Article history:
Received 16 April 2015
Received in revised form
5 June 2015
Accepted 20 June 2015
Available online 29 June 2015

Keywords:
Dye desalting
Electrodialysis
Acid blue 9
Monovalent anion selectivity
Dye–membrane interaction
Fouling.

ABSTRACT

Currently nanofiltration predominates the membrane application of dye desalting and purification, and it is very effective to produce low-salt dye from raw dye with high inorganic salt impurities. However it is difficult and costly to produce dye products with ultralow impurities, because the desalting performance decreases proportionally as the concentration of salt impurity decreases. Here in this study, an optimized electrodialysis desalting process was proposed to fill the gap. The dye–membrane interactions, fouling mechanism and abatement strategy were carefully investigated and well understood. Long term system performance stability and reasonable process cost are achieved. Nearly all SO_4^{2-} in the feed dye can be removed, and residual [Cl^-] is only 130 mg/L (~96% removal) in the final aqueous dye product (~200 g/L). The overall purification cost is $0.097/kg as dye solids, which is very economically competitive. The electrodialysis desalting process proposed here provides another feasible and competitive approach for dye desalting and purification other than nanofiltration.

1. Introduction

Multi-color inkjet printing is very popular nowadays, which is usually based on the CMYK (refers to the four inks used: cyan, magenta, yellow and black) color model [1]. Inkjet dyes are highly concentrated colorants specially designed for this printing process, and they should have high purity and very low salt content to increase ink stability as well as to reduce the corrosion to the metal parts in the printers [2,3]. Most dyes are produced by chemical synthesis, while this synthesis process produces byproduct salts (typically NaCl and Na_2SO_4) as impurities [4]. Nanofiltration (NF) based processes are widely used for dye desalting and purification [4–12]. The rejection is low for small molecules (molecular weight < 150 Da) and ions (especially monovalent anions), but is high for big molecules such as typical dye molecules (molecular weight > 400 Da) in typical NF processes [4]. By carefully screening the membranes with appropriate pore diameters (slightly larger than conventional NF membranes, which are also known as loose NF or tight Ultrafiltration), salts with divalent anions (such as Na_2SO_4) can also be separated from the aqueous dyes [10]. Thus, the NF based processes are widely used for the removal of byproduct salts, which is able to produce aqueous dye with more than 25% dye content and less than 1% byproduct salt [4]. Particularly, NF process is very efficient to remove impurities in raw aqueous dye products with high byproduct salts. However the NaCl removal flux decreases greatly as the salt concentration decreases in dye solution [4]. For example, producing salt-free aqueous dye (~0.025% NaCl) from low-salt dye (~0.5% NaCl) is as costly as producing low-salt aqueous dye (~0.5% NaCl) from high salt dye (~10% NaCl). Because of the high cost for further desalting in NF based process, most dye-stuff producers in China provide raw dye (high byproduct salts) and low-salt dye products only. Other low cost dye desalting technologies are needed for the production of salt free dye products, especially for the inkjet dyes.

Electrodialysis (ED) is another mature desalting technology, in which ions are transferred through ion exchange membranes (IEMs) by means of a DC electric field [13]. The cost of ED process relies on the salt concentration in feed solution, which decreases significantly as the salt concentration decreases [14]. And it is well recognized that ED is more economically efficient than pressure driven membrane processes (such as NF) for low-salt concentration (< 0.5%) feed solutions [14]. So ED is promising as an alternative to NF, especially to produce salt-free aqueous dye from low-salt dye. ED technology had been evaluated for dye desalting in previous literatures [15–17]. Meininger et al. [15] removed alkali and alkaline earth metal halides from aqueous dye solutions by electrodialysis. Voss from BASF [16] proposed a desalting process based on ED by acidifying the dye solutions first. Majewska-Nowak

* Corresponding author. Fax: +86 577 86689300.
E-mail address: weiming@iccas.ac.cn (W.-M. Zhang).

http://dx.doi.org/10.1016/j.memsci.2015.06.027
0376-7388/

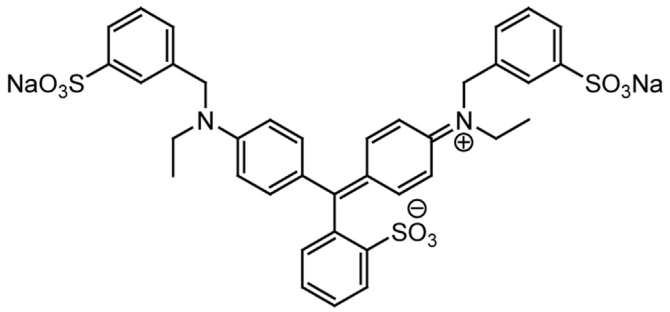

Scheme 1. Molecular structure of AB9. The molecular formula is $C_{37}H_{34}N_2Na_2O_9S_3$, and the molecular weight is 792.85 g/mol. The peak absorption wavelength is 628 nm.

[17] performed laboratory tests to determine the efficiency of dye solution desalination by electrodialysis, and it was found that the separation efficiency was strongly dependent on the dye molecular weight. Although such efforts were made to understand the feasibility of the dye desalting by ED, the dye–membrane interactions were not very clear in these processes. Dye molecules are usually ionized as anions (for all acid dyes, as well as some reactive dye and direct dyes) or cations (for all basic dyes and some direct dyes), and the affinities between the dye ions and the IEMs are very strong. These affinities caused serious membrane contamination during the desalting process, long process time, high energy consumption, as well as short membrane life.

Acid blue 9 (AB9, C.I. Number 42090) is one of the standard cyan inkjet dyes [2], and it is widely used for multi-color inkjet printing and other applications such as swimming pool water and foodstuffs [18]. The molecular structure of AB9 is presented in Scheme 1, which exists as divalent anion [19] in neutral and slightly basic aqueous solutions. In the current work, an ED based dye desalting process was proposed and tested to produce salt-free aqueous AB9 from low-salt products. The dye–membrane interactions, fouling mechanism and abatement strategy were carefully investigated and well understood. Long term system performance stability and reasonable process cost were achieved. The ED process here is proven to be another feasible and competitive approach for dye desalting and purification other than NF.

2. Materials and methods

2.1. Analytical methods

Low-salt AB9 solid products were obtained from Shuanghong Chemical Co., Ltd., China. Standard AB9 samples were prepared by further diafiltration and concentration of the above raw dye solution (dissolved with deionized water) with tight UF (UH004 membrane with molecular weight cutoff (MWCO) of 4000 Da, obtained from MICRODYN-NADIR GmbH, Germany) [10,12]. The purified AB9 solution was then dried at 70 °C in a vacuum oven for about 24 h to get the standard sample. The concentrations of the AB9 in aqueous dye were determined by monitoring the absorbance at 628 nm on a Shimadzu UV-2450 UV–vis spectrophotometer.

The Cl^- concentrations in aqueous AB9 solutions were analyzed by potentiometric titration (INESA ZDJ-4B automatic titrator) with Ag electrode. The aqueous dye samples were acidified with HNO_3 first, then titrated with 0.1 mol/L $AgNO_3$ standard solution. The SO_4^{2-} concentrations were determined by potentiometric titration with 0.05 mol/L $Pb(NO_3)_2$ solutions and Pb^{2+} ion selective electrode in water-ethanol mixtures. The H^+ and OH^- concentrations were also analyzed by potentiometric titration. All chemicals (A.R. grade) and electrodes for the titration were purchased from Sinopharm Chemical Reagent Co, Ltd., China.

The cumulative current efficiency η in the ED process is calculated by the amount of Na^+ increase in concentrate stream or Na^+ decrease in diluate stream. Because of the lower initial Na^+ concentration, it is easier to determine the changes of Na^+ concentrations in concentrate in the current work. So the current efficiency is defined as the following formula:

$$\eta = \frac{[Na^+]_t V_t - [Na^+]_0 V_0}{Q_t} \quad (1)$$

where V is the volume of the product solution, $[Na^+]$ is the Na^+ concentration in concentrate solution, and Q is the cumulative charge transferred in moles of electrons. The subscript "0" and "t" represent the sampling points, namely "before the test" and "at sampling point t", respectively.

The permselectivity between SO_4^{2-} and Cl^- ions in AEMs (also called the transport number of SO_4^{2-} relative to Cl^- ions) is defined as the following formula: [20]

$$P_{Cl}^{SO4} = \frac{t_{SO4}/t_{Cl}}{c_{SO4}/c_{Cl}} = \frac{\Delta c_{SO4}/\Delta c_{Cl}}{\bar{c}_{SO4}/\bar{c}_{Cl}} \quad (2)$$

where t_{SO4} and t_{Cl} are the transport numbers of SO_4^{2-} and Cl^- ions in the AEMs, and c_{SO4} and c_{Cl} are the equivalent concentrations of SO_4^{2-} and Cl^- ions in the desalting chambers (diluate) in the ED process, respectively. In this work, real time transport numbers are not available and averages between two adjacent sampling points are used, and the equation can be formulated as the right form. Δc is the decrease of ion concentrations, and $\bar{c}$ is the average concentration in diluate solution during the sampling period.

2.2. Sulfate removal procedure

It is difficult to remove divalent anions, such as sulfate, from the AB9 solution in this study. So a sulfate removal procedure was conducted before the ED desalting process. Firstly, low-salt AB9 powders were carefully dissolved. The precise concentration of sulfate in this solution was determined by potentiometric titration with $Pb(NO_3)_2$. Then stoichiometric amount of $BaCl_2 \cdot 2H_2O$ solids were added to AB9 solutions under stirring. After the sulfate were completely precipitated (~60 min), the solution was filtrated by a flat sheet ultrafiltration (UF) membrane (0.22 μm).

2.3. The ED system

Simplified illustration and photograph of the ED system used in this study are shown in Fig. 1. The detailed configurations of the stack were well documented in our previous works [21]. The spacer used has a dimension of 260 mm (length) × 130 mm (width) × 0.9 mm (thickness), with an effective area of 187 cm^2. The arrangement of ED stack is shown in Fig. 1a. It has two-compartment configuration with co-current flows, which consists of alternating anion-exchange membranes (AEMs, JAM-II, 4–8 Ω cm^2, 200 μm) and cation exchange membranes (CEMs, JCM-II, 4–8 Ω cm^2, 200 μm). There are four repeating cell pairs in the stack. All membranes were obtained from Beijing Tingrun Membrane Technology Development Co. Ltd., China. NaCl solution (5000 mg/L) was chosen as electrode rinses, and NaCl (1000 mg/L) was prepared as concentrate stream to receive the salt impurities. Low-salt AB9 aqueous solution (200 g/L) was circulated as diluate stream. The volume of each solution is 1.0 L. All streams in the ED stack are driven by a four-channel metering pump (LEAD-2, from Baoding Longer Precision Pump Co., Ltd., China), and the flow rate of each stream is adjusted to 9.6 L/h (corresponding flow velocity in stack is 2.2 cm/s). The ED stack is operated basically in a

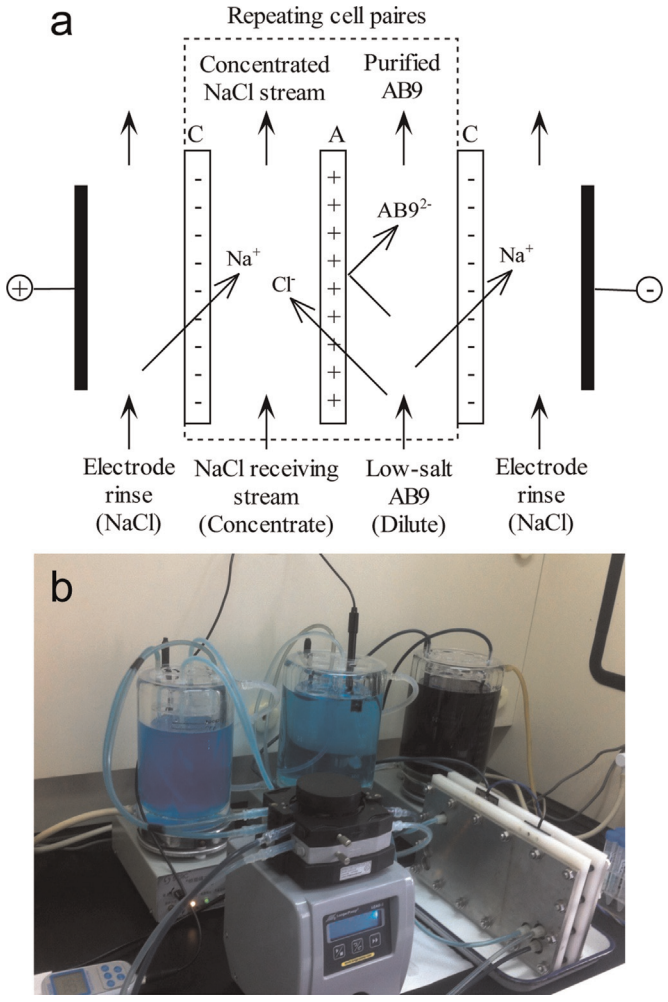

Fig. 1. Experimental setup of the ED system. (a) Illustration of the ED stack used for AB9 desalting. A, anion exchange membrane; C, cation exchange membrane. (b) Photograph of the running system in lab.

constant current (0.50 A, namely 2.7 mA/cm^2) mode. The AEMs and CEMs selectively permeate anions and cations under the electric field, respectively. Acid blue 9 is an anionic disodium salt. While because of the large ion radii of AB9 anions (~11 Å, from CambridgeSoft Chem3D 8.0), there are much more obstructions to permeate through the AEMs (illustrated in Fig. 1a). So it is theoretically feasible to selectively remove salt impurities such as NaCl from the low-salt AB9 solutions.

3. Results and discussion

3.1. Monovalent anion selectivity

Potentiometric titration results show that the concentrations of Cl^- and SO_4^{2-} in AB9 solution (200 g/L) are 21 mmol/L and 36 mmol/L, respectively. So a simple mixture of NaCl and Na_2SO_4 with equivalent concentrations (1.0 L) was used as diluate solution to evaluate the ED performance first. Basically the stack was operated in a constant current (0.50 A, corresponding current density is 2.7 mA/cm^2) mode, and the stack voltage was limited within 12 V. Tap water heat exchanger was utilized to stabilize the solution temperatures in all circulations. Some parameters including stack voltage, current, solution temperature and charge transferred were monitored by our homemade control system [22,23]. Samples were taken at predetermined intervals (every 0.025 mol

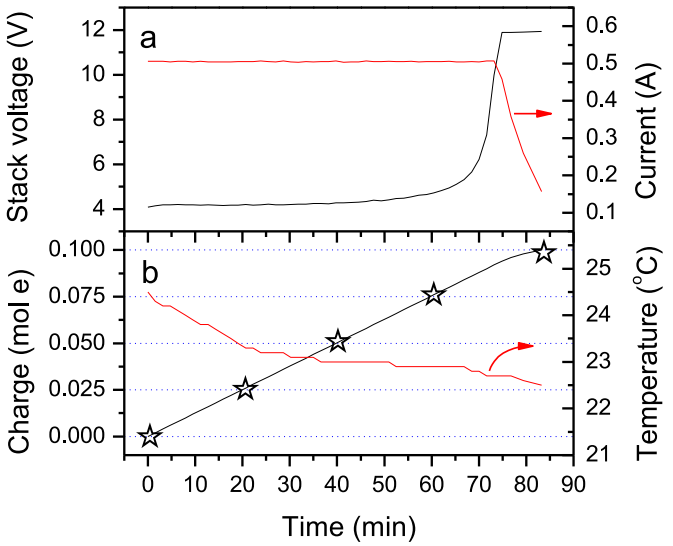

Fig. 2. Online data profile of the ED process with NaCl and Na_2SO_4 mixture. (a) Stack voltage and current curves. (b) Total charge transferred in the stack and diluate solution temperature curves, the sampling points are marked as star symbols (☆) herein. The ED stack here is newly assembled with brand new membranes.

electrons) for off-line analysis during the testing. The online profile recorded by our control system is shown in Fig. 2. The initial stack voltage and current are stable at 4 V and 0.5 A for a long time, respectively. The initial stack resistance is about 8 Ω. The stack voltage increases swiftly at the last period (> 70 min) of the test, and it reaches the voltage limit quickly. After that the stack current declines quickly, indicating that the stack resistance increases further. The charge transferred can be readily calculated by the current profile, which is represented in Fig. 2b. The temperature variation in the diluate tank is also shown here, which indicates that the solution temperature is quite stable (22.5–24.5 °C). In addition, pH of both diluate and concentrate keep neutral during the whole test. Corresponding offline analysis results are shown in Fig. 3. The concentrations of Cl^- and SO_4^{2-} decrease linearly in diluate solution, and increase linearly in concentrate solution as the charge transferred in stack increases (Fig. 3a). The

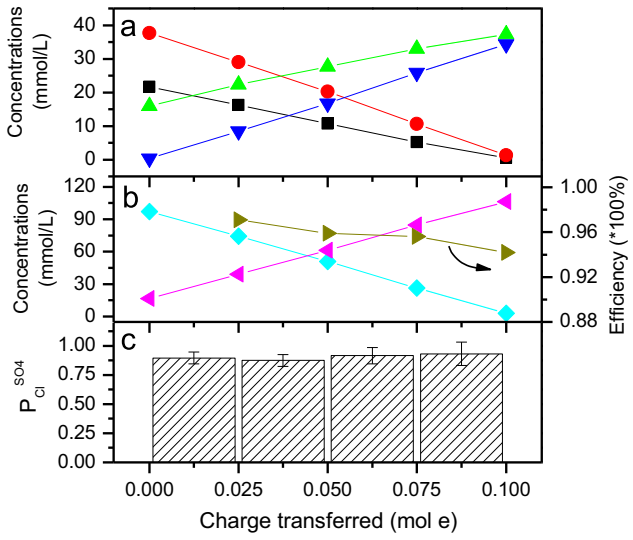

Fig. 3. Offline sample analysis results with NaCl and Na_2SO_4 mixture during the ED process. (a) Anion concentration variations. $[Cl^-]$ (■) and $[SO_4^{2-}]$ (●) in diluate solution; $[Cl^-]$ (▲) and $[SO_4^{2-}]$ (▼) in concentrate solution. (b) $[Na^+]$ in diluate solution (◆) and in concentrate solution (◀), and cumulative current efficiencies (▶). (c) The permselectivity between SO_4^{2-} and Cl^- ions in AEMs.

linearity in the concentration change pattern indicates that the ED stack works well. The Na^+ concentrations in both diluate and concentrate solutions can be calculated by charge balance, which are also linear and are demonstrated in Fig. 3b. The total charge transferred in this work is small (0.1 mole/L), and the solution volume variations are negligible. So volumes of all solutions are regarded constant in this study. The cumulative current efficiencies can be calculated according to Eq. (1), and are also shown in Fig. 3b. All current efficiencies are retained high (94–97%), and a slight decline is observed because the back diffusion increases as the diluate concentration decreases and as the concentrate concentration increases. The existence of two kinds of anions (Cl^- and SO_4^{2-}) leads to a competition of transfer in AEMs. The AEM permselectivity between SO_4^{2-} and Cl^- ions is calculated from the concentration variations of Cl^- and SO_4^{2-} in Fig. 3a according to Eq. (2), and the results can be found in Fig. 3c. The permselectivity nearly keeps constant and the values are pretty close to 1 (0.88–0.93), which indicates that the JAM-II AEM nearly has no selectivity between SO_4^{2-} and Cl^- ions here (very little Cl^- selective).

However, the permselectivity is very different in AB9 direct desalting process. The ED desalting process was repeated with low-salt AB9 solution (~200 g/L, 1.0 L), and all other parameters were identical with previous test with simple NaCl and Na_2SO_4 mixture. The online data profile is shown in Fig. 4. Although the concentrations of Cl^- and SO_4^{2-} impurities in AB9 solution are the same as those in previous test, the stack voltage is obviously higher (Fig. 4a). The stack voltage increases steeply as the ED test begins (from 5 to 9 V in 3 min), and then increases to 12 V (the voltage limit) after 58 min. It means that the existence of AB9 dye anions significantly increases the stack resistance. The diluate solution temperature and charge transferred curves are shown in Fig. 4b, which are similar to those in previous test. The sampling points are also marked in Fig. 4b, and the offline analysis results are represented in Fig. 5. It is clearly shown in Fig. 5a that the $[Cl^-]$ decreases much swifter than $[SO_4^{2-}]$. The $[Cl^-]$ decrease from 21.5 mmol/L to 3.2 mmol/L (85% removal), while the $[SO_4^{2-}]$ only decrease from 36.4 mmol/L to 31.5 mmol/L (13% removal) after the desalination process. Significant water splitting is observed in the current test, which is very different from previous running (no water splitting is observed, and pH of both diluate and concentrate

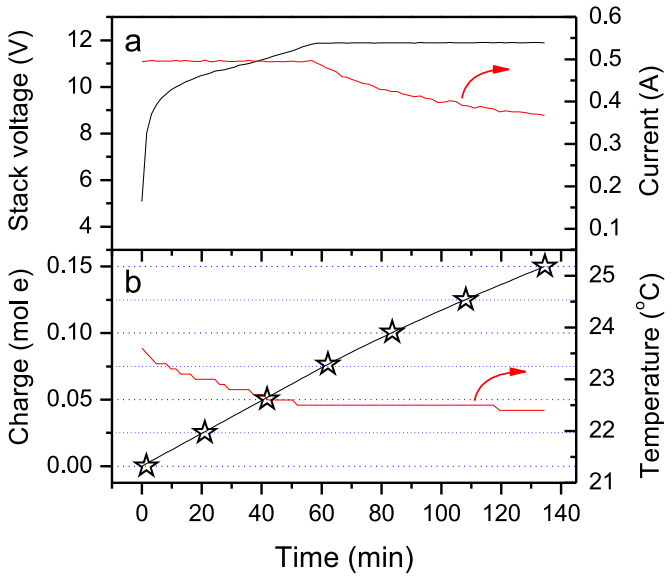

Fig. 4. Online data profile of the direct AB9 desalting process by ED. (a) Stack voltage and current curves. (b) Total charge transferred in the stack and diluate solution temperature curves. The sampling points are marked as star symbols (☆).

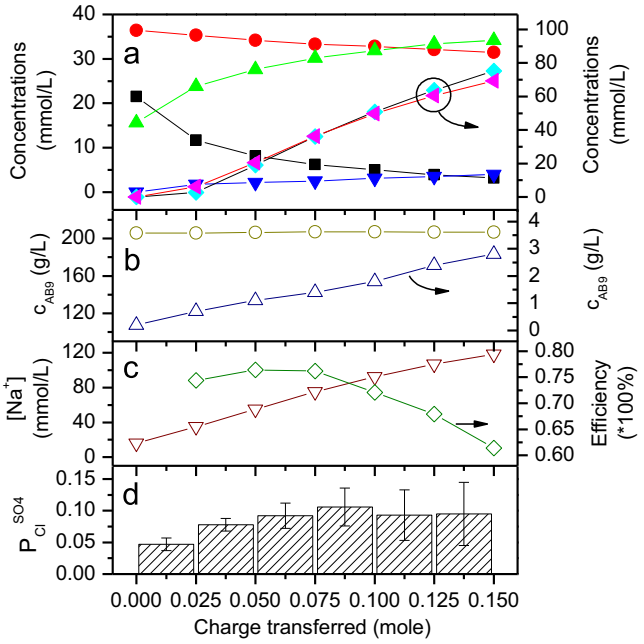

Fig. 5. Offline sample analysis results of direct AB9 desalting by ED. (a) Ion concentration variations. $[Cl^-]$ (■), $[SO_4^{2-}]$ (●) and $[H^+]$ (◆) in feed AB9 solution (the diluate); $[Cl^-]$ (▲), $[SO_4^{2-}]$ (▼) and $[OH^-]$ (◀) in NaCl receiving solution (the concentrate). (b) AB9 concentrations in feed AB9 solution (○) and in NaCl receiving solution (△). (c) $[Na^+]$ in NaCl receiving solution (▽) and cumulative current efficiencies (◇). (d) The permselectivity between SO_4^{2-} and Cl^- ions in AEMs.

keep neutral in previous running with simple mixture of NaCl and Na_2SO_4). The diluate (AB9 solution) becomes acidic and the concentrate (the NaCl receiving solution) becomes alkaline during the test. The concentration variations of $[H^+]$ in diluate and $[OH^-]$ in concentrate are also shown in Fig. 5a. It is shown that the water splitting is negligible at the beginning of the test (charge transferred less than 0.025 mole), and then the concentrations of $[H^+]$ and $[OH^-]$ increase to about 70 mmol/L equally at the end. The AB9 leakage is also evaluated and shown in Fig. 5b. The AB9 concentration keeps constant in the dye feed solution (206–208 g/L in all samples), and increases monotonously to 2.8 g/L in concentrate solution. These results indicate that the maximum leakage ratio is as low as 1.4% in the process. The $[Na^+]$ variations can be readily calculated from the concentrations of all anions in concentrate stream, and the cumulative current efficiencies are calculated according to Eq. (1). Both of the results can be found in Fig. 5c. Reasonable current efficiencies are maintained in the first half of the test (74–76%), and then drop to 61.4% at the end of the test. The current efficiency decline is likely to be attributed to the increases of $[H^+]$ in diluate and $[OH^-]$ in concentrate, respectively. Because leakage of co-ions are much more significant for H^+ (in AEMs) and OH^- (in CEMs), the back diffusion increases and causes decline of current efficiency. The AEM permselectivity between SO_4^{2-} and Cl^- ions is calculated likewise, and the results are shown in Fig. 5d. The low permselectivity of SO_4^{2-} to Cl^- ions (0.05–0.10) indicates that the AEMs are much more selective (10–20 times) to Cl^- than SO_4^{2-}, which is entirely different from the results of previous ED test without AB9. Namely, the JAM-II AEMs obtain abnormal monovalent ion permselectivity when AB9 is involved in the diluate solution.

The dramatic changes in permselectivity of JAM-II AEMs must be related to some changes of their microcosmic structures. The ED stack was flushed with plenty of water and disassembled immediately after the test, and the changes of membranes were carefully investigated. The CEMs remain the same, and no change in appearance is observed. On the contrary, the AEMs changed a

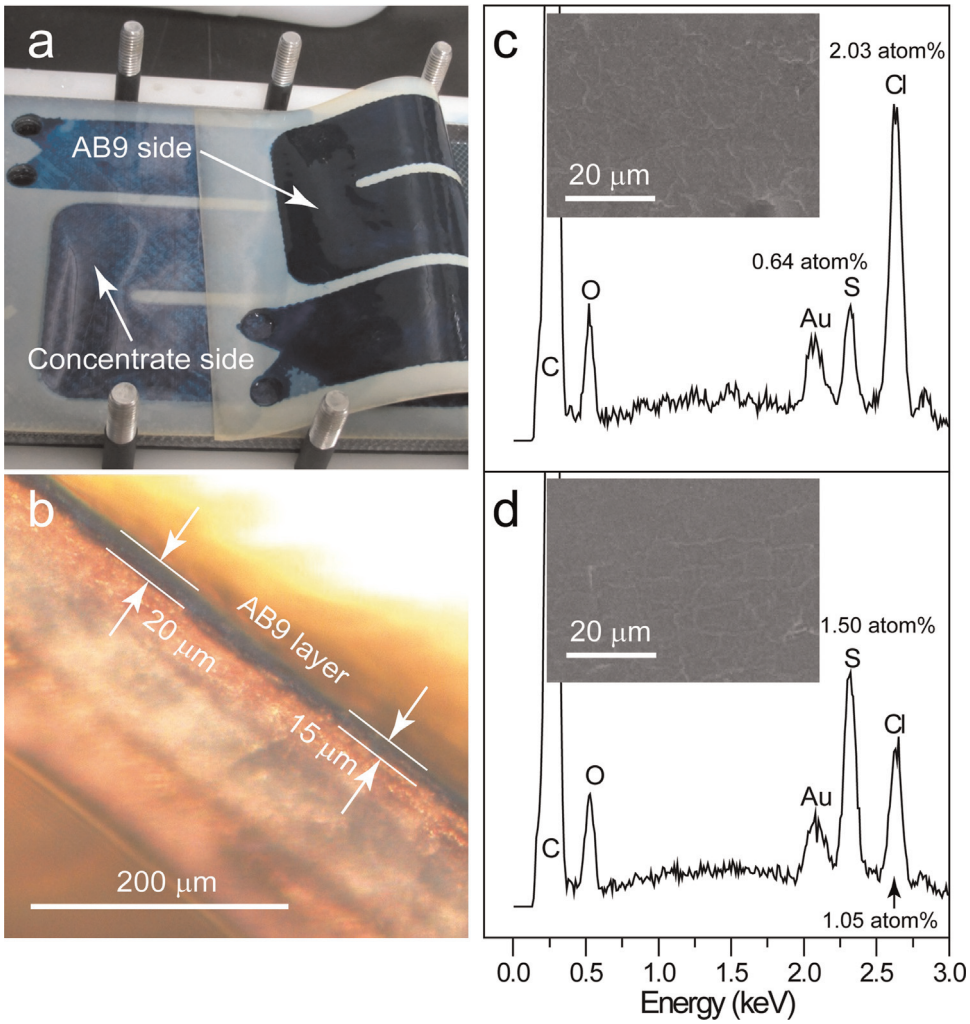

Fig. 6. The adsorption of dye on AEM surfaces after the ED process. (a) Photograph of an AEM in the disassembled stack after the desalting process. (b) Optical microscope image on the cross section of AEM. EDX spectrums of the AEM surfaces on concentrate side (c) and AB9 side (d), and element Cl and S compositions are marked. The Au signals are originated from Au sputtering in sample pretreatment. SEM images of the corresponding membrane spots are also shown as insets. (For interpretation of the references to color in this figure, the reader is referred to the web version of this article.)

lot after the desalting process. Fig. 6a is a photograph of the AEM in the disassembled stack, the colors of the two sides are apparently different. The cathodic surface (the AB9 side) is dark blue and the anodic surface (the concentrate side) is much paler in color. The AEMs are semi transparent with milky color before the ED test, which is also presented in Fig. 6a (AEM parts sealed by the spacer). An optical microscope image on the cross section of the AEM is shown in Fig. 6b. The AB9 molecules adsorb on the cathodic surface, while the other surface is much less affected. In order to further understand the surface adsorptions of AB9 on both sides of the AEMs, energy-dispersive X-ray (EDX) spectrum is utilized and the results are shown in Fig. 6c–d. The signal of element Cl is significantly higher than element S on the anodic side (concentrate side, 0.64 atom% for element S and 2.03 atom% for element Cl) of AEM, indicating little AB9 (containing 3 sulfonic acid groups) and SO_4^{2-} ions exist on this surface. While in the cathodic surface, the situation is much different. The signal of element S is higher than element Cl (AB9 side, 1.50 atom% for element S and 1.05 atom% for element Cl). Because the AEM membranes are highly permeable for small inorganic anions such as SO_4^{2-}, the surface concentration of SO_4^{2-} should be comparable on both sides. So the signal of element S here should come from AB9, which means that plenty of AB9 adsorb on this surface (about 50% of the Cl^- are replaced by AB9). The AB9 adsorption layer here is negatively charged, so all anions have to overcome the electrostatic repulsion force with this layer before permeating through the AEM. The repulsion force of monovalent anions such as Cl^- is much weaker than that of divalent and multivalent anions, which is the reason why the AEMs obtain monovalent ion permselectivity when AB9 is involved [24–26].

The water splitting also takes place on these surfaces. There are only two possible places for water splitting in our ED stack: anodic surfaces of CEMs and cathodic surfaces of AEMs. Since the water splitting on anodic surfaces of CEMs causes acidification of concentrate stream (which is opposite to our experimental results), the only possibility is cathodic surfaces of AEMs (the AB9 side). The stack voltages are 12 V in ED tests with and without AB9, the voltage drop across the AEM should be similar. No water splitting is observed in the ED test with simple mixture of NaCl and Na_2SO_4, while significant water splitting occurs in the ED test with AB9 solution (NaCl and Na_2SO_4 exist as byproduct salts). These observations indicate that the water splitting is facilitated. The AB9 adsorption layer is negatively charged, which locates on the original positively charged AEM surface. This structure is somewhat similar to that of a bipolar membrane, which can be attributed to the facilitation of water splitting.

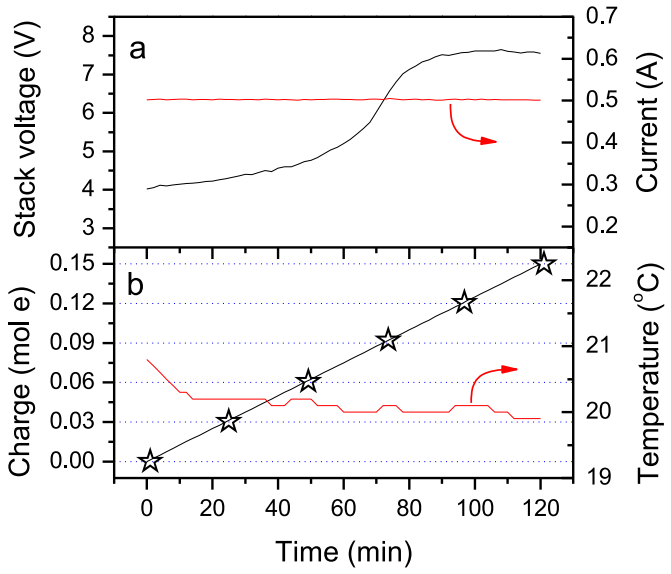

Fig. 7. Online data profile of the AB9 desalting process by ED after removing SO_4^{2-} by $BaCl_2$. (a) Stack voltage and current curves. (b) Total charge transferred in the stack and diluate solution temperature curves. The sampling points are marked as star symbols (☆).

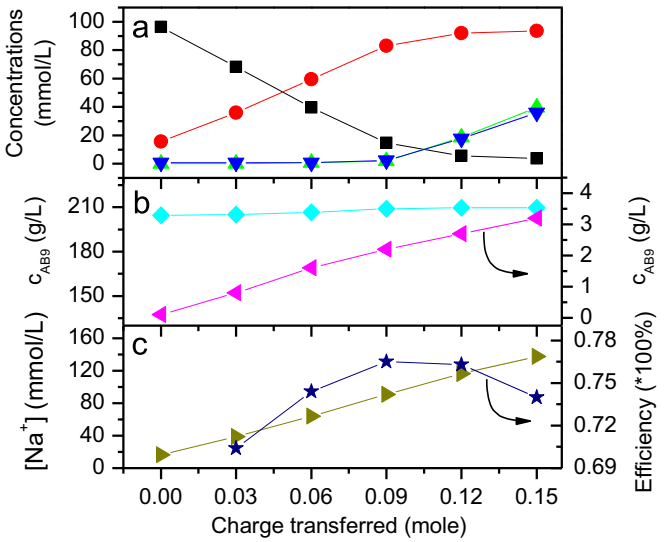

Fig. 8. Offline sample analysis results of AB9 desalting by ED after removing SO_4^{2-} by $BaCl_2$. (a) Ion concentration variations. $[Cl^-]$ (■) and $[H^+]$ (▲) in feed AB9 solution (the diluate); $[Cl^-]$ (●) and $[OH^-]$ (▼) in NaCl receiving solution (the concentrate). (b) AB9 concentrations in feed AB9 solution (◆) and in NaCl receiving solution (◀). (c) $[Na^+]$ in NaCl receiving solution (▶) and cumulative current efficiencies (★).

3.2. 3.2. Optimized ED process with $BaCl_2$ precipitation

As discussed previously in Section 3.1, it is not feasible to remove SO_4^{2-} impurity directly from the AB9 solution by ED because the dye anions adsorb on the AEM surfaces and form monovalent anion selective layers. So a sulfate removal procedure with $BaCl_2$ precipitation was proposed, and described in Section 2.2. After the precipitation and filtration, all SO_4^{2-} are completely replaced by Cl^- ions (about 93 mmol/L in total). The residual $[Ba^{2+}]$ in the dye solution is not detectable (<0.5 mg/L, namely 3.6×10^{-6} mol/L) by ICP-OES, and the residual $[SO_4^{2-}]$ is less than 0.5 mmol/L (<50 mg/L) in the resulted AB9 solution ($\sim$200 g/L). The ED desalting process was repeated with this AB9 solution, and all other parameters were identical with previous tests. Fig. 7 shows the online data profile of the testing. The stack is operated in a constant current (0.50 A, namely 2.7 mA/cm^2) mode, and the stack voltage is also limited within 12 V (never reach the upper limit). The initial stack voltage is only about 4 V and it increases slowly (Fig. 7a), which is very similar to that in the test of simple mixture of NaCl and Na_2SO_4 (see Fig. 2a), and is significantly lower than that in the direct desalting of low-salt AB9 solution (see Fig. 4a). The temperature variation in the diluate tank (AB9 solution) is shown in Fig. 7b, and the solution temperature is also stable (19.9–20.8 °C). The total charge transferred in the stack is also shown in Fig. 7b. Samples were taken at predetermined intervals (every 0.03 mol electrons, namely every 24 min at a constant current of 0.50 A), and the corresponding offline sample analysis results are shown in Fig. 8. The $[Cl^-]$ variations in both streams are stacked in Fig. 8a. It is clear that the $[Cl^-]$ decreases in diluate and increases in concentrate linearly before the total charge transferred reaches 0.09 mol electrons (before 72 min). In this period there is little water splitting occurred in the stack, because both the $[H^+]$ in diluate and $[OH^-]$ in concentrate are almost zero (Fig. 8a). While after this sampling point (0.09 mol electrons, namely 72 min), the slope of the $[Cl^-]$ variations declines, and significant water splitting is observed. These results indicate that before this sampling point, the $[Cl^-]$ is high enough (>14.7 mmol/L) to support all current density (2.7 mA/cm^2) in the AEMs (see Fig. 1a). While after that point, the $[Cl^-]$ decreases and no longer to be able to support that current density. The stack voltage curve in Fig. 7a further verifies this conclusion. The stack voltage increases steeply from 60 min (5.2 V) to 80 min (7.2 V), this rapid voltage increase matches the emergence of water splitting perfectly. The AB9 leakage is also shown in Fig. 8b, and the result is nearly identical with that in direct AB9 desalting process (see Fig. 5b). The AB9 concentration keeps constant in the dye feed solution (205–210 g/L in all samples), and the AB9 concentration in concentrate solution increases monotonously to 3.2 g/L (maximum leakage ratio of 1.5%). The $[Na^+]$ in the NaCl receiving solution (the concentrate) can be readily calculated by the concentration of all anions (Cl^-, $AB9^{2-}$ and OH^-), and the result is shown in Fig. 8c. The $[Na^+]$ increase is almost linear. The cumulative current efficiencies can be calculated according to Eq. (1), and are also shown in Fig. 8c. Reasonable current efficiencies (70–76%) are maintained during the process. Because the $[H^+]$ and $[OH^-]$ caused by water splitting is lower than that in AB9 direct desalting process, the final current efficiencies don't drop a lot (different from Fig. 5c).

The $[Cl^-]$ decreases from 96.4 to 3.7 mmol/L (namely 3400 to 130 mg/L as Cl^-), and the $[H^+]$ increases from 0 to 39.7 mmol/L. The H^+ can be eliminated by adding concentrated NaOH solution to the product until the pH reaches 7. The residual NaCl is only 3.7 mmol/L (216 mg/L as NaCl) in our AB9 (210 g/L) product solution, which meets the specification of salt-free products for ink-jet applications.

3.3. Membrane clean strategy

In order to better understand the process stability, the optimized AB9 desalting was repeated in multiple batches. The final product specifications, including concentrations of AB9, H^+ and Cl^-, are reproduced in later batches; nevertheless, the stack voltage increases significantly. The stack voltage curves of the first 3 consecutive batches (labeled as Run 1–3) are represented in Fig. 9a. It is shown that the initial stack voltage increases from 4.0 V to 6.0 V after three runs, indicating a remarkable increase of membrane resistance. Previously we had disassembled the stack after AB9 desalting process, and found that all CEMs remain unchanged but the cathodic surfaces (the AB9 side) of AEMs are contaminated by AB9 anions (see Fig. 6 for details). The increase in

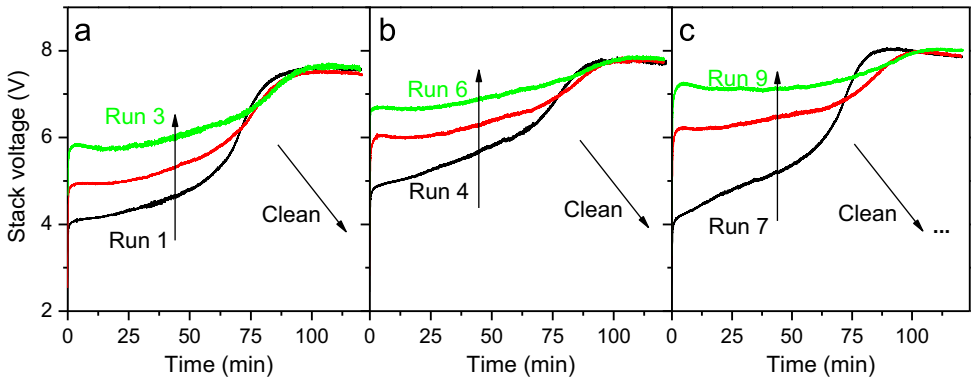

Fig. 9. Stack voltage profiles of multiple AB9 desalting by ED after removing SO_4^{2-} by $BaCl_2$, including run 1–3 (a), Run 4–6 (b) and Run 7–9 (c). A clean procedure was involved after every 3 continuous run.

stack resistance is very likely related to this dye–AEM interaction. In Fig. 6b, we can find that the AB9 anions not only adsorb on the cathodic surfaces of AEMs, but also slightly enter into the AEM matrix. These AB9 anions take the place of Cl^- as counter anions in the AEM matrix near cathodic surfaces, which results in a blue region with a thickness of 15–20 μm. It is clear that the AB9 anions have difficulty in permeating through the AEMs. Actually homogeneous IEMs are not completely dense, and they have hydrated pathway channels regulated by cross-linked chains and the fixed ions [13]. The diameter of these channels are very limited, for example the AC-220 membranes (ASTOM Co. Ltd., Japan) have a MWCO of 300 [27]. Large anions, such as $AB9^{2-}$ (746.85 g/mol, and larger in aqueous solution because of hydration), may be "stuck" in these channels and hinder the permeation of other small anions (such as Cl^-) in the AEM matrix. The more AB9 anions are "stuck" in the AEM, the more difficult for other anions to permeate through the membrane. In order to renew the anion permeability of the AEM, these "stuck" AB9 anions must be removed.

Fortunately the major affinity is ionic bonds between the acid dye molecules and the AEMs, and this interaction is reversible. A clean procedure was proposed to renew the anion permeability. First, the stack was flushed with tap water thoroughly to remove all highly concentrated dye solutions. Then NaCl solutions (about 5000 mg/L, 1.0 L) were used as diluate and concentrated solutions. The stack was first operated in normal mode (same current direction as AB9 desalting) at the same current density (0.5 A stack current, 2.7 mA/cm^2), and the stack voltage profile is shown in Fig. 10. The stack voltage is as high as 10.7 V, and it decreases gradually to 8.3 V after 10 min. However, when the polarity of DC current is reversed (opposite to the AB9 desalting), the stack voltage decreases suddenly and stabilizes at 5.1 V quickly. This dramatic decrease of stack resistance is attributed to the removal of the AB9 anions from the AEM matrix, because it is much easier for these AB9 anions to move back and exit than to permeate through the AEM matrix. The clean operation was repeated by fresh NaCl solutions, and the stack voltage decreases gradually from 4.9 V to 3.9 V during the following normal operation, and it decreases suddenly to 3.4 V during the following reverse operation (in 5000 mg/L NaCl solutions). This stack voltage is pretty close to that of a brand new stack without any dye contaminations (about 3.0 V, and the voltage drop on electrodes is as high as 2.50 V according to our previous work in NaCl rinse system [21]), which indicates that the AEMs are successfully renewed for anion permeability. The stack voltage decreases after the clean procedure, and long term process stability can be achieved. Fig. 9 shows the stack voltage profiles of nine runs, and a clean procedure is performed after every three consecutive runs. The stack voltages are pretty stable in these tests.

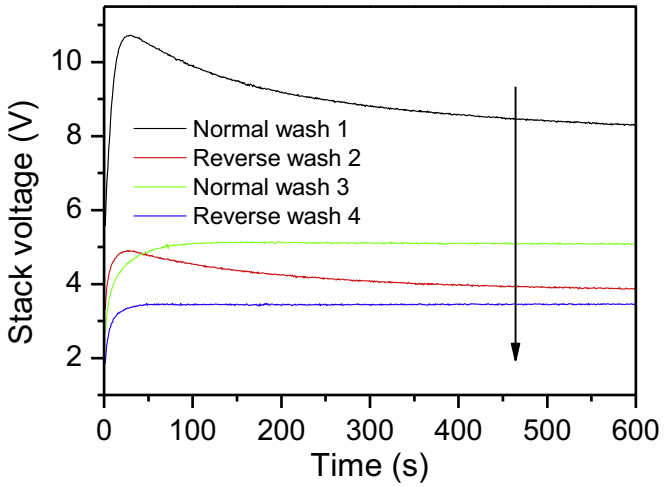

Fig. 10. Stack voltage profiles in a typical clean procedure (after run 3).

The fouling states of the AEMs before and after the clean procedure are further characterized by EDX (shown in Fig. 11). The cross-section SEM image of the AEM after three consecutive runs is shown in Fig. 11a, and the thickness of the membrane is about 200 μm. The consequent EDX line scan results of element S and Cl are shown in Fig. 11b and c, respectively. The EDX line scan curves of element S and Cl are perfectly complementary, because the total equivalent concentration of anions (Cl^- and $AB9^{2-}$) in the AEM is constant (related to the ion exchange capacity). The S content is lower near the anodic surface and higher near the cathodic surface, which is opposite to that of element Cl. The higher element S signal near the cathodic surface indicates that AB9 anions have entered into the AEM matrix and have taken the place of Cl^-. The AB9 contamination depth is about 50 μm, which is also marked in Fig. 11b and c. After the clean procedure, similar characterizations are carried out. The cross section SEM image of AEM is shown in Fig. 11d, and the line scan curves of element S and Cl are shown in Fig. 11e and f. The depth of AB9 contaminated area decreases significantly, which is about 20 μm (also marked in Fig. 11e and f). The significant shrinkage of AB9 fouled regions indicates that the clean procedure here is effective to remove AB9 anions in the AEM matrix, naturally decreasing the membrane resistance and renewing the anion permeability of the AEMs.

3.4. Brief cost analysis

The AB9 desalting process proposed in this study consists of three subprocesses. Firstly, SO_4^{2-} in the low-salt AB9 feed solution need to be removed with $BaCl_2$ precipitation. Secondly, these

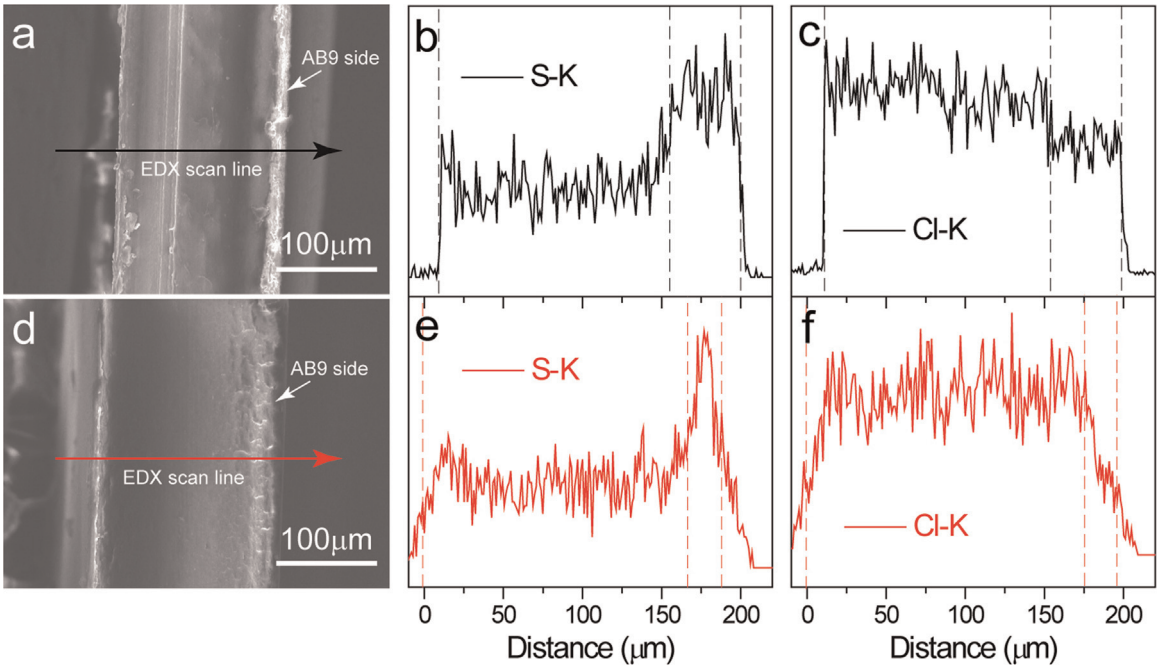

Fig. 11. Comparison of AEM cross sections before (a–c) and after (d–f) the clean procedure. (a) SEM image of the membrane before the clean. (b) EDX line scan of element S. (c) EDX line scan of element Cl. (d) SEM image of the membrane after the clean. (e) EDX line scan of element S. (f) EDX line scan of element Cl.

sulfate removed solution are desalted to remove NaCl impurity by ED. At last, a post treatment must be involved because the AB9 solution is acidic and the NaCl receiving solution is basified. The overall process cost depends on the total cost of these sub-processes. The detailed cost estimations of all subprocesses are provided in Table S1 in supporting information, which is straightforwardly based on the prices of chemicals and process parameters in our experimental study. The overall purification cost (from low-salt to salt-free product) is \$0.097/kg as AB9 solids. The capital cost of ED system (60%) predominates in the overall cost, and the chemical cost of $BaCl_2 \cdot 2H_2O$ (23%) is the second important portion. The market price of the low-salt AB9 in this study is \$14/kg as solids, and the price of salt-free product is as high as \$25/kg. Because of the huge added valve, the ED desalting process proposed in this study is very economically competitive.

4. Conclusions

Conventional ED technology was utilized for AB9 desalting, and the dye–membrane interactions were carefully investigated. Strong affinities between AB9 anions and the positively charged AEMs drive the dye molecules not only adsorb on the AEM surfaces, but also move into the AEM matrix. The relative large molecule size results in difficulty for AB9 to permeate through the membrane and be "stuck" near the cathodic surfaces, and they take the place of Cl^- as counter ions in the AEM matrix. This dye fouling layer exhibits unusual monovalent anion selectivity, and increases the electric resistance of the membrane. It was also found that the AB9 fouling layers were able to be removed partially in fresh NaCl solutions when applied a reversed DC current, and long term system performance stability can be achieved. All these hypotheses have been verified by the ED process data and membrane characterization results. Based on the above findings, an optimized ED process was proposed to produce salt-free AB9 from low-salt dye product. Nearly all SO_4^{2-} in the feed AB9 can be removed (from 36 mmol/L to <0.5 mmol/L), and residual [Cl^-] is only 130 mg/L (from 93 mmol/L to 3.7 mmol/L, ~96% removal). The overall purification cost is \$0.097/kg as AB9 solids, which is very economically competitive. The ED desalting process proposed here opens a new door to dye desalting and purification other than NF. Especially for the desalination of the low-salted dyestuff, the ED technology demonstrates good performance and economic advantage..

Acknowledgments

The authors are grateful for financial support by the National Natural Science Foundation of China (Project nos. 21203139 and 21003097).

Appendix A. Supplementary materials

Supplementary data associated with this article can be found in the online version at 10.1016/j.memsci.2015.06.027.

References

[1] S. Jennings, Artist's Color Manual: The Complete Guide to Working with Color, Chronicle Books, San Francisco (2003), p. 21.
[2] Inkjet Dyes. ⟨http://www.dyes-pigments.com/inkjet-dyes.html⟩ (accessed 8.12.14).
[3] P.C. Pistorius, G.T. Burstein, Growth of corrosion pits on stainless steel in chloride solution containing dilute sulphate, Corros. Sci. 33 (1992) 1885–1897.
[4] S. Yu, C. Gao, H. Su, M. Liu, Nanofiltration used for desalination and concentration in dye production, Desalination 140 (2001) 97–100.
[5] K. Majewska-Nowak, M. Kabsch-Korbutowicz, T. Winnicki, Salt effect on the dye separation by hydrophilic membranes, Desalination 108 (1997) 221–229.
[6] C. Crossley, How the dye industry is benefiting from membrane technology, Filtr. Sep. 39 (2002) 36–38.
[7] G. Yang, W. Xing, N. Xu, Concentration and diafiltration of aqueous fluorescent whitener solution by nanofiltration, Desalination 150 (2002) 155–164.
[8] I. Koyuncu, D. Topacik, Effects of operating conditions on the salt rejection of nanofiltration membranes in reactive dye/salt mixtures, Sep. Purif. Technol. 33 (2003) 283–294.
[9] P. Mikulášek, V. Kopecký, O. Kušnierik, Salt removal from process solutions in liquid dye production by nanofiltration, Desalination 200 (2006) 409–410.
[10] Y. He, G. Li, H. Wang, J. Zhao, H. Su, Q. Huang, Effect of operating conditions on

separation performance of reactive dye solution with membrane process, J. Membr. Sci. 321 (2008) 183–189.
[11] E. Alventosa-deLara, S. Barredo-Damas, E. Zuriaga-Agustí, M.I. Alcaina-Miranda, M.I. Iborra-Clar, Ultrafiltration ceramic membrane performance during the treatment of model solutions containing dye and salt, Sep. Purif. Technol. 129 (2014) 96–105.
[12] J. Lin, W. Ye, H. Zeng, H. Yang, J. Shen, S. Darvishmanesh, P. Luis, A. Sotto, B. Van der Bruggen, Fractionation of direct dyes and salts in aqueous solution using loose nanofiltration membranes, J. Membr. Sci. 477 (2015) 183–193.
[13] H. Strathmann, Electrodialysis, a mature technology with a multitude of new applications, Desalination 264 (2010) 268–288.
[14] R.W. Baker, Membrane Technology and Applications, 2nd ed., John Wiley & Sons Ltd., Chichester (2004), p. 222.
[15] F.D. Meininger, K.D. Opitz, J.D. Semel, Process for the manufacture of aqueous, fluid preparations of reactive dyes with a low salt content, Europe Patent, 0167107, 1988.
[16] H. Voss, Removal of salts by electrodialysis, U.S. Patent, 5282939, 1994.
[17] K.M. Majewska-Nowak, Treatment of organic dye solutions by electrodialysis, Membr. Water Treat. 4 (2013) 203–214.
[18] J. Wang, H. Wang, Clean production of Acid Blue 9 via catalytic oxidation in water, Ind. Eng. Chem. Res. 48 (2009) 5548–5550.
[19] A.R. Khataee, V. Vatanpour, A.R. Amani Ghadim, Decolorization of C.I. Acid Blue 9 solution by UV/Nano-TiO_2, Fenton, Fenton-like, electro-Fenton and electrocoagulation processes: a comparative study, J. Hazard. Mater. 161 (2009) 1225–1233.
[20] T. Sata, Ion Exchange Membranes: Preparation, Characterization, Modification and Application, Royal Society of Chemistry, Cambridge (2004), p. 137.
[21] Q. Chen, Y.-Y. Liu, C. Xue, Y.-L. Yang, W.-M. Zhang, Energy self-sufficient desalination stack as a potential fresh water supply on small islands, Desalination 359 (2015) 52–58.
[22] Q. Chen, C. Xue, W.-M. Zhang, W.-G. Song, L.-J. Wan, K.-S. Ma, Green production of ultrahigh-basicity polyaluminum salts with maximum atomic economy by ultrafiltration and electrodialysis with bipolar membranes, Ind. Eng. Chem. Res. 53 (2014) 13467–13474.
[23] J.-X. Zhuang, Q. Chen, S. Wang, W.-M. Zhang, W.-G. Song, L.-J. Wan, K.-S. Ma, C.-N. Zhang, Zero discharge process for foil industry waste acid reclamation: coupling of diffusion dialysis and electrodialysis with bipolar membranes, J. Membr. Sci. 432 (2013) 90–96.
[24] Y. Mizutani, Ion exchange membranes with preferential permselectivity for monovalent ions, J. Membr. Sci. 54 (1990) 233–257.
[25] T. Sata, Studies on anion exchange membranes having permselectivity for specific anions in electrodialysis—effect of hydrophilicity of anion exchange membranes on permselectivity of anions, J. Membr. Sci. 167 (2000) 1–31.
[26] G. Chamoulaud, D. Bélanger, Chemical modification of the surface of a sulfonated membrane by formation of a sulfonamide bond, Langmuir 20 (2004) 4989–4995.
[27] G. Atungulu, S. Koide, S. Sasaki, W. Cao, Ion-exchange membrane mediated electrodialysis of scallop broth: Ion, free amino acid and heavy metal profiles, J. Food Eng. 78 (2007) 1285–1290.